Experimental evaluation of optimized ablation patterns for laser refractive surgery

Carlos Dorronsoro[1,*], Laura Remon[1], Jesús Merayo-Lloves[2] and Susana Marcos[1]

[1]*Instituto de Optica "Daza de Valdés", Consejo Superior de Investigaciones Científicas, Serrano 121, 28006, Madrid, Spain*

[2]*Instituto de Oftalmobiología Aplicada, Universidad de Valladolid Campus Miguel Delibes, 47011 Valladolid, Spain*

[*] *cdorronsoro@io.cfmac.csic.es*

http://www.vision.csic.es

Abstract: A new experimental model based on plastic (Filofocon A) artificial eyes was used to study the ablation profiles and the outcomes of three state-of-the-art refractive surgery excimer lasers provided with narrow-beam flying spot and optimized algorithms (Ladarvision 4000, Alcon; Technolas 217 Z100, Bausch&Lomb; Allegretto wave Eye-Q, Wavelight). The 3-D ablation patterns produced by myopic laser corrections (-9, -6 and -3 D) on flat and spherical surfaces of Filofocon A were measured using high resolution optical profilometry. We found significant differences across lasers in the shape and depth of the ablation patterns. A comparison of the ablation patterns on flat and on spherical surfaces provided a measurement of the laser efficiency losses from the center to the periphery at each point of the spherical plastic corneas. This effect also varied across lasers, depending on their fluence (120-400 mJ/cm^2). Estimates of the post-operative corneal shapes were obtained from the measurement on Filofocon A and plastic-corneal tissue correction factors. The predicted post-operative corneal ablation shape, ablated volume, asphericity and spherical aberration varied across lasers, as well as the relative contribution of ablation pattern designs and efficiency losses to the increased asphericity. Although the results show that the algorithms have been optimized to reduce the induction of spherical aberration, they would still benefit from the application of correction factors for efficiency effects derived from a systematic approach using experimental plastic models. These models have proved useful (1) to assess the outcomes of different lasers or ablation algorithms, (2) for precise calibration and testing of the lasers, and (3) to calculate experimental correction factors for efficiency effects.

OCIS codes: (170.1020) Ablation of tissue; (170.3890) Medical optics instrumentation; (330.5370) Physiological optics; (330.4460) Ophthalmic optics; (220.1000) Aberration compensation.

References and links

1. M. Mrochen, M. S. Eldine, M. Kaemmerer, T. Seiler, and W. Hutz, "Improvement in photorefractive corneal laser surgery results using an active eye-tracking system," J. Cataract. Refract. Surg. **27**, 1000-1006 (2001).
2. T. Kohnen, "Classification of excimer laser profiles," J. Cataract. Refract. Surg. **32**, 543-544 (2006).
3. T. Kohnen, "Reshaping the cornea: Which laser profiles should we use?," J. Cataract. Refract. Surg. **34**, 1225-1225 (2008).
4. E. Moreno-Barriuso, J. Merayo-Lloves, S. Marcos, R. Navarro, L. Llorente, and S. Barbero, "Ocular aberrations before and after myopic corneal refractive surgery: LASIK-induced changes measured with Laser Ray Tracing," Invest. Ophthalmol. Vis. Sci. **42**, 1396-1403 (2001).
5. S. Marcos, B. Barbero, L. Llorente, and J. Merayo-Lloves, "Optical response to LASIK for myopia from total and corneal aberration measurements," Invest. Ophthalmol. Vis. Sci. **42**, 3349-3356 (2001).

#111696 - $15.00 USD Received 20 May 2009; revised 27 Jul 2009; accepted 3 Aug 2009; published 14 Aug 2009

6. M. Mrochen, M. Kaemmerer, and T. Seiler, "Wavefront-guided Laser in situ Keratomileusis: Early results in three eyes.," J. Refract. Surg. **16**, 116-121 (2000).
7. T. Kohnen, C. Kuhne, and J. Buhren, "The future role of wavefront-guided excimer ablation," Graefes Arch. Clin. Exp. Ophthalmol. **245**, 189-194 (2007).
8. P. Padmanabhan, M. Mrochen, S. Basuthkar, D. Viswanathan, and R. Joseph, "Wavefront-guided versus wavefront-optimized laser in situ keratomileusis: Contralateral comparative study," J. Cataract. Refract. Surg. **34**, 389-397 (2008).
9. M. V. Netto, W. Dupps, and S. E. Wilson, "Wavefront-guided ablation: Evidence for efficacy compared to traditional ablation," Am. J. Ophthalmol. **141**, 360-368 (2006).
10. J. L. Alio, and R. Montes-Mico, "Wavefront-guided versus standard LASIK enhancement for residual refractive errors," Ophthalmology **113**, 191-197 (2006).
11. A. Perez-Escudero, C. Dorronsoro, L. Sawides, L. Remon, J. Merayo-Lloves, and S. Marcos, "Minor influence of Myopic Laser In Situ Keratomileusis on the Posterior Corneal Surface," Invest. Ophthalmol. Vis. Sci. iovs.09-3411 (2009).
12. W. J. Dupps, and S. E. Wilson, "Biomechanics and wound healing in the cornea," Exp. Eye Res. **83**, 709-720 (2006).
13. M. Mrochen, and T. Seiler, "Influence of corneal curvature on calculation of ablation patterns used in photorefractive laser surgery.," J. Refract. Surg. **17**, S584-S587. (2001).
14. S. Marcos, D. Cano, and S. Barbero, "Increase of corneal asphericity after standard myopic LASIK surgery is not inherent to the Munnerlyn algorithm," J. Refract. Surg. **19**, 592-596 (2003).
15. R. G. Anera, J. R. Jimenez, L. Jimenez del Barco, and E. Hita, "Changes in corneal asphericity after laser refractive surgery, including reflection losses and nonnormal incidence upon the anterior cornea," Opt. Lett. **28**, 417-419 (2003).
16. J. R. Jimenez, R. G. Anera, L. Jiménez del Barco, and E. Hita, "Effect on laser-ablation algorithms of reflection losses and nonnormal incidence on the anterior cornea," Appl. Phys. Lett. **81**, 1521-1523 (2002).
17. D. Cano, B. Barbero, and S. Marcos, "Comparison of real and computer-simulated outcomes of LASIK refractive surgery.," J. Opt. Soc. Am. A. **21**, 926-936 (2004).
18. D. Gatinel, T. Hoang-Xuan, and D. Azar, "Determination of corneal asphericity after myopia surgery with the excimer laser: a mathematical model," Invest. Ophthalmol. Vis. Sci. **42**, 1736-1742 (2001).
19. S. Arba-Mosquera, and D. de Ortueta, "Geometrical analysis of the loss of ablation efficiency at non-normal incidence," Opt. Express **16**, 3877-3895 (2008).
20. Y. Kwon, M. Choi, and S. Bott, "Impact of ablation efficiency reduction on post-surgery corneal asphericity: simulation of the laser refractive surgery with a flying spot laser beam," Opt. Express **16**, 11808-11821 (2008).
21. J. R. Jimenez, R. G. Anera, L. J. del Barco, E. Hita, and F. Perez-Ocon, "Correction factor for ablation algorithms used in corneal refractive surgery with gaussian-profile beams," Opt. Express **13**, 336-343 (2005).
22. J. R. Jimenez, R. G. Anera, L. J. del Barco, and E. Hita, "Influence of laser polarization on ocular refractive parameters after refractive surgery," Opt. Lett. **29**, 962-964 (2004).
23. J. D. Gottsch, E. V. Rencs, J. L. Cambier, D. Hall, D. T. Azar, and W. J. Stark, "Excimer laser calibration system," J. Refract. Surg. **12**, 401-411 (1996).
24. C. B. Odonnell, J. Kemner, and F. E. Odonnell, "Surface roughness in PMMA is linearly related to the amount of excimer laser ablation," J. Refract. Surg. **12**, 171-174 (1996).
25. A. M. Roszkowska, G. Korn, M. Lenzner, M. Kirsch, O. Kittelmann, R. Zatonski, P. Ferreri, and G. Ferreri, "Experimental and clinical investigation of efficiency and ablation profiles of new solid-state deep-ultraviolet laser for vision correction," J. Cataract. Refract. Surg. **30**, 2536-2542 (2003).
26. S. Marcos, C. Dorronsoro, and D. Cano, "Spherical aberration prevention method in e.g. laser refractive surgery system," (Patent WO 2005/122873 A1, 2005).
27. C. Dorronsoro, D. Cano, J. Merayo, and S. Marcos, "Experiments on PMMA models to predict the impact of corneal refractive surgery on corneal shape," Opt. Express **14**, 6142-6156 (2006).
28. J. Buehren, "The effect of the asphericity of myopic laser ablation profiles on the induction of wavefront aberrations," in *Wavefront Congress* (Alicante, Spain, 2009).
29. ANSI Z80.11 Laser Systems for Corneal Reshaping (American National Standard Institute, 2007).
30. B. Drum, "Evaluating the Safety and Effectiveness of "Aberration-Free" Ophthalmic Refractive Surgery," in 9th Annual FDA Science Forum (Washington, DC, 2003).
31. B. Drum, "Radial efficiency function in refractive surgery: Ablation losses caused by corneal curvature," in 11th annual FDA Science Forum (Washington, DC, 2005).
32. C. Dorronsoro, J. Siegel, L. Remon, and S. Marcos, "Suitability of Filofocon A and PMMA for experimental models in excimer laser ablation refractive surgery," Opt. Express **16**, 20955-20967 (2008).
33. L. Llorente, B. Barbero, J. Merayo, and S. Marcos, "Changes in corneal and total aberrations induced by LASIK surgery for hyperopia.," J. Refract. Surg. **20**, 203-216 (2004).
34. R. Artigas, F. Laguarta, and C. Cadevall, "Dual-technology optical sensor head for 3D surface shape measurements on the micro- and nanoscales," O. Wolfgang, and T. Mitsuo, eds. (SPIE, Strasbourg, France, 2004), pp. 166-174.

#111696 - $15.00 USD Received 20 May 2009; revised 27 Jul 2009; accepted 3 Aug 2009; published 14 Aug 2009

35. S. H. Goods, R. M. Watson, and M. Yi, "Thermal Expansion and Hydration Behavior of PMMA Molding Materials for LIGA Applications," (Sandia National Laboratories, Albuquerque, New Mexico, 2003).
36. S. Barbero, S. Marcos, J. Merayo-Lloves, and E. Moreno-Barriuso, "Validation of the estimation of corneal aberrations from videokeratography in keratoconus," J. Refract. Surg. **18**, 263-270 (2002).
37. B. T. Fisher, and D. W. Hahn, "Development and numerical solution of a mechanistic model for corneal tissue ablation with the 193 nm argon fluoride excimer laser," J. Opt. Soc. Am. A **24**, 265-277 (2007).
38. J. Noack, R. Tonnies, K. Hohla, R. Birngruber, and A. Vogel, "Influence of ablation plume dynamics on the formation of central islands in excimer laser photorefractive keratectomy," Ophthalmology **104**, 823-830 (1997).

1. Introduction

Refractive surgery has become a popular procedure to correct the refractive errors of the eye. The procedure has been improved over the past years, thanks to the refinement of the involved technologies: flying spot lasers, pupil trackers [1], microkeratomes. Optical outcomes have also benefited from the improvement in the ablation pattern design. Current ablation algorithms are wavefront-optimized or customized to the patients' optical aberrations (aspheric, wavefront-guided or topography-guided) [2, 3], with the aim of avoiding the increase of spherical aberration that was a major issue with standard ablation profiles [4, 5].

One goal of current refractive surgery is the correction of higher optical aberrations of the eye, and not only conventional refractive errors, although there is still some controversy regarding correcting higher order aberrations in virgin eyes. Customized wavefront guided surgery is assisted by wavefront sensors and topographers (to measure optical aberrations) and precise lasers, which are now available in clinical sites. However, despite some initial promising results and some evidence that the increase of spherical aberration is attenuated [6], there is still an important lack of predictability of post-operative high-order aberrations in wavefront-guided refractive surgery, and in many cases spherical aberration is still introduced[7]. Although some studies show trends toward better visual and optical outcomes following wavefront-customized procedures, the improvement is hardly significant when compared with the new generation of conventional procedures [8-10]. Many causes have been pointed out for the relatively minor impact of aberration correction [7], as fluctuations in the aberrations or errors in their measurement, centration, alignment or torsion errors (during the measurements or the ablation), and flap creation effects. Corneal biomechanics is another potential cause for the inaccurate prediction of the corneal postoperative shape. While several studies have shown changes in the posterior corneal surface suggesting an influence of corneal biomechanical effects in the optical outcomes, recent work [11] shows that the shape of the posterior cornea is practically unaffected in LASIK. In any case, the biomechanical response of the cornea after tissue removal and wound healing are added effects to physical effects that compromise the predictability and stability of refractive surgery [12].

Undoubtedly, the ablation pattern design and how accurately it is transferred to the cornea (i.e. physical aspects of the ablation process) determine the optical outcomes. In particular, ablation efficiency effects, caused by energy losses as the ablating spot moves from the center to the periphery of the cornea, have been identified as a cause of the increase of spherical aberration [13]. The combination of standard ablation patterns with ablation efficiency effects have been studied in detail analytically [14-18] and numerically [19, 20], with an increasing degree of sophistication including effects such as the spot shape [21], polarization [22], pulse overlap, realistic eye-tracking and intermediate states of the ablated cornea. However, all of these models are highly dependent on the approximations of the physical mechanisms and assumptions of the parameters of the model. Presumably, the subsequent improvements of the ablation patterns with the estimated correction factors are now included in the proprietary ablation algorithms of most laser platforms.

Plastic models have been used in refractive surgery research and calibration for a long time, especially for the assessment of roughness and calibration of fluence [23-25]. However, it has not been until recently that plastic models have been used to study in detail the shape changes induced by refractive surgery on flat and spherical surfaces [26-28]. Ablating plastic model corneas (not affected by biomechanical or other biological effects) with clinical lasers,

#111696 - $15.00 USD Received 20 May 2009; revised 27 Jul 2009; accepted 3 Aug 2009; published 14 Aug 2009

in combination with pre- and post- operative shape assessment, allows to measure directly the actual ablation pattern provided by the laser, avoiding several of the approximations and assumptions used in theoretical models. In addition, different laser platforms or different algorithms can be compared experimentally. The procedure also allows the measurement of ablation efficiency effects, or the effect of laser decentrations. Plastic models are also interesting for quality assessment and market approval of new laser platforms [29-31], to check experimentally the calibration state of individual laser units and the diagnosis of adjustment problems. They will also help to validate theoretical models of refractive surgery [19, 20].

Plastic models are not intended to mimic the response of the cornea. They are used to characterize the laser system, and in particular the density of spots at each point, to obtain accurate predictions in cornea. The ideal material for plastic models should have optical and ablation properties that produce a linear response to the laser pulses at all points. Furthermore, in order to extrapolate the results obtained in plastic to corneal tissue, precise measurements of the ablation properties of the material are needed [32]. Filofocon A is a novel material with optical and ablation properties that make it more suitable than PMMA, the material traditionally used for refractive surgery research, as reported in a recent study [32]. The use of Filofocon A in combination with clinical lasers has not been reported before.

In this work we describe a new design for Filofocon A model eyes, including a new eye support that improves alignment. Flat and spherical artificial eyes were ablated with three different clinical lasers, provided with different optimized algorithms. The shape of the surfaces was measured with high resolution optical profilometry. Evaluation of the ablation profiles on flat surfaces allowed us to test the actual ablation pattern programmed into the laser system, differences across lasers, and possible miscalibrations of the laser units. Ablations on spherical surfaces allowed assessing changes in asphericity after refractive surgery. A comparison of the ablation profiles on spherical surfaces and identical ablations on flat surfaces allows quantifying geometry-related ablation efficiency losses. Once the differences in ablation and optical properties between plastic and corneal tissue are considered, it is possible to estimate the correction factor for efficiency effects for corneal tissue, and the relative contribution of physical factors affecting the post-operative corneal shape. Although efficiency losses are more important in PTK or hyperopic profiles [26, 33], myopic procedures are much more common, and larger clinical databases are available for myopic than for hyperopic LASIK. Consequently, we chose myopic algorithms because the study of these patterns across lasers would have a larger impact in the clinical practice.

Although the results are obtained for particular laser systems, the understanding of the physics of the ablation in curved surfaces, and the methodology described can be generalized to design better ablation algorithms, not only for refractive surgery, but also for related areas, as customized contact lens manufacture.

2. Methods

2.1. Lasers

Table 1 shows the three laser platforms used in this study, provided with state-of-the-art optimized algorithms. All lasers used flying-spot technology, and were Argon Fluoride (ArF) excimer lasers (193 nm emission wavelength) delivering nanosecond-pulses. Fluence, repetition rate, and spot shapes and diameters varied across lasers. The optical zone was set to 6.5 mm in all cases.

2.2. Artificial eyes

The artificial eyes consisted on plastic cylinders of Filofocon A [32], with a diameter of 12.7 mm, finished either on a polished flat or spherical (7.8-mm nominal radii of curvature) surface. All eyes had an artificial iris (6.5 mm aperture) located 3.5 mm behind the artificial cornea. The artificial iris is formed by a groove painted on its anterior surface. The nominal eye length was 24.65 mm in all eyes, so that the back focal plane of the spherical surfaces is

#111696 - $15.00 USD Received 20 May 2009; revised 27 Jul 2009; accepted 3 Aug 2009; published 14 Aug 2009

near the back surface -also polished- of the cylinder. The artificial eyes were manufactured by MedLens, INC, Front Royal, VA, USA. The first surface was re-polished in a precision optics lathe to ensure high surface precision (individually assessed on a profilometer, section 2.4) before the ablations. To define the orientation of the artificial corneas, they were marked at the edge with a 1-mm length meridional line. Figure 1(a) shows a photograph of two of the artificial eyes of the study. A total of 40 Filofocon eyes (20 flat and 20 spherical) were ablated under different conditions during the study.

The artificial eyes were placed in a support (see Fig. 1(b)) that consists of a CMOS chip (from a webcam) acting as an artificial retina, a tip and tilt platform (for both the eye and the CMOS chip), and a tunable filter. The pixel position of the CMOS chip corresponding to the center of the cylinder was previously calibrated and considered as the artificial fovea. The artificial fovea and the artificial pupil define the line of sight of the artificial eye, which can be oriented using the tip and tilt platform.

Table 1. Laser platforms used in this study. (Nominal data from www.fda.gov)

	Alcon LADAR Vision	Bausch & Lomb Technolas 217Z100	Wavelight Allegretto EyeQ
Algorithm	Standard	Zyoptix Tissue Saving	F-CAT
Peak Fluence (mJ/cm^2) Average Fluence	400 210	120	400 200
Repetition Rate	100 Hz	100 Hz	400 Hz
Spot Shape Spot Diameter (mm)	Gaussian 0.95	Truncated G. 1 and 2	Gaussian 0.95
Optical Zone	6.5 mm		
Ablation Zone	8 mm	9.6 mm	8 mm
Eye tracker	Disabled		
Wavelength	193 nm		

2.3. Ablation protocol with clinical lasers

The artificial eyes were ablated in the different operating rooms where the clinical lasers were located, and the full experimental procedure supervised by the investigators. The lasers were fine-adjusted and calibrated by each company's technical support experts before each session. During the ablations, the lasers were operated by the surgeon or the operating room assistants in charge at each clinic. All standard procedures were followed except for the eye tracker that was disabled (and thus the pupil centered manually). The optical zone was set to 6.5 mm. The ablation patterns selected were: Zyoptix Tissue Saving for the Technolas 217 Z100, Standard algorithm for the LADAR-vision and F-CAT for the Allegretto Eye-Q.

An additional procedure was needed to align the artificial eye to the laser. Each clinical laser has a different fixation stimulus, typically a collimated laser beam (red line in Fig. 1 (b)). The alignment requires the superposition of that stimulus beam with the eye's line of sight (green line in Fig. 1 (b)). In practice, this involves bringing the stimulus (imaged on the CMOS sensor through the artificial eye) to the fovea (reference pixel), by adjusting the tip and tilt platform. To avoid image saturation of the fixation spot, the intensity of the fixation stimuli was adjusted with a tunable filter. The filter was moved aside during ablation. After fixation adjustment, pupil centration was achieved as in patients. The presence of multiple colinear reflexes confirmed the correct centration and alignment of the eye.

Pairs of flat and spherical artificial eyes were always ablated consecutively (see Fig. 2, and Media 1), under identical conditions (correction, algorithm, calibration state, centration and alignment). Right before each pair (flat/sphere) of myopic corrections, the laser fluence was checked (and calibrated if needed), and the alignment adjusted.

Five pairs of clinical ablations (on flat and spherical surfaces) were performed for each laser. Three pairs of refractive surgery procedures were performed with -9 D corrections, one pair with -6 D and one pair with -3 D. As the F-CAT algorithm (Wavelight) has adjustable

#111696 - $15.00 USD Received 20 May 2009; revised 27 Jul 2009; accepted 3 Aug 2009; published 14 Aug 2009

target asphericity, with this laser we ablated two sets of artificial corneas with two different values of the parameter Q: Q=0 and 0.25.

We checked (using a thermosensitive sheet) that the differences in laser vergence from the center to the periphery were negligible. Therefore the ablations on flat surfaces should not be affected by non-normal incidence.

2.4. Pre- and Post- operative measurements

An optical profilometric microscope [34] (PLμ, Sensofar, Barcelona, Spain), mounted on a vibration-isolated table, was used to measure the shape of the first surface of the artificial eyes both before and after the ablations. The slit-confocal configuration of the instrument was used to measure the surface height at each point, in an "extended shape" custom measurement mode. At each point, a pattern of parallel lines is projected with a 100x microscope onto the surface while a CCD camera images the reflected lines, through the same optics. The instrument scans the sample in the Z direction, changing the focus position of the lines relative to the surface being measured. Image processing algorithms retrieve the Z point at which the reflected image of the parallel lines is sharpest, which is considered the height of the surface at that point. To obtain the shape of the artificial corneas, 1148 points of a rectangular grid covering the central 11 millimeters of the surface were measured.

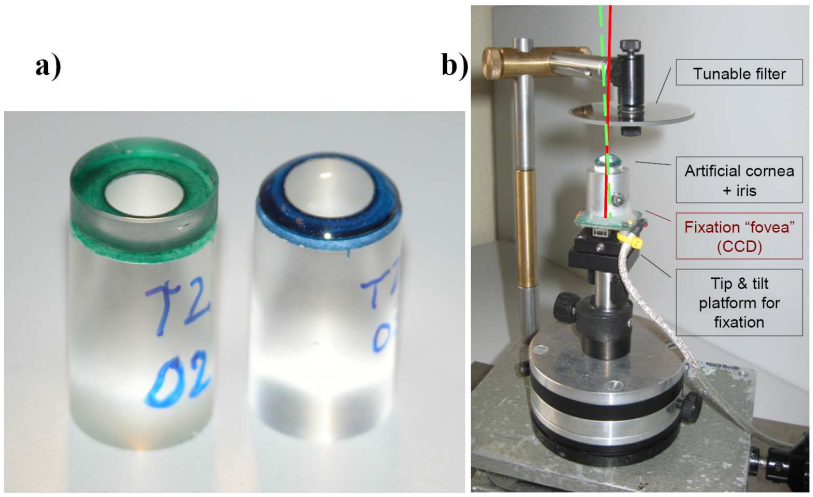

Fig. 1. (a) Artificial eyes of Filofocon A (flat and spherical). (b) Artificial eye support. The red line represents the fixation stimulus of the laser, while the green line represents the line of sight of the eye. Aligning means to make both axes coincident.

Prior to the measurement, the artificial corneas were rotated until the reference mark was oriented along the y-axis of the microscope. The corneal apex, found using the 20x interferometric objective on the same instrument, was used as the origin for the measurements in the curved surfaces. In the case of flat surfaces, the apex was taken as the center of the cylinder (pre-operative) or the center of the ablation (postoperative).

Measurements on spherical corneas were more demanding than on flat corneas, due to the steep slope at the periphery causing two undesired effects: on the one hand, fewer projected lines are in focus on the sample at the same time, and on the other hand the intensity of the back-reflected light is relatively low. Custom algorithms were developed as part of the measurement procedure definition, including the calculation of a confidence index for each point measured. Additional tests were performed to estimate the optimal measurement parameters and the significance thresholds (used to discard invalid points).

Each surface measurement took around 4 hours. As dilation of the sample during the measurement is a potential cause of error, the laboratory temperature was monitored and controlled, and the samples were stored near the measurement instrument.

#111696 - $15.00 USD Received 20 May 2009; revised 27 Jul 2009; accepted 3 Aug 2009; published 14 Aug 2009

All the spherical artificial corneas were measured before and after the ablation. All flat corneas were measured after the ablation. Only a few pre-operative flat corneas were measured, as the deviation from flatness was as low as the precision of the instrument (1 μm peak to peak for the whole surface).

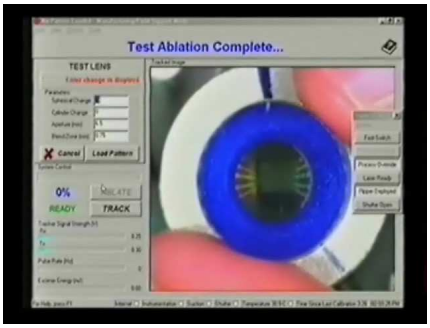

Fig. 2. Single-frame excerpt from video recordings (Media 1) of a refractive surgery procedure in a flat plastic artificial cornea of Filofocon A.

2.5. Data analysis

2.5.1. Extracting the ablation patterns

We wrote routines in Matlab (Mathworks, Nantick, MA, USA) to extract the laser ablation patterns from the shape measurements.

Flat Surfaces

The topographies measured on ablated flat surfaces should represent the actual spot density profile delivered by the laser. The measurements were only corrected numerically for the tilt found on the non-ablated area. This tilt appears in the measurement because the line of sight of the eye is not necessarily aligned with the microscope optical axis. We found tilts typically lower than 2 degrees. These tilts come from the topography measurement and not from the ablation, where the alignment and centration of the artificial eye were well controlled. We tested the procedure by measuring the same sample at different slight tilting angles, and checking that tilt was correctly compensated by the software.

Spherical surfaces

The ablation pattern was also obtained from the ablated spherical corneas by subtracting a base sphere (corresponding to the pre-operative spherical surface) from the measured elevation. We found that subtracting the analytical surface produced a better estimation (less noise) than a point-by-point subtraction of elevation maps.

2.5.2. Computing the laser efficiency effects

The efficiency effects are described by the ablation efficiency factor *K*, depending on the incidence angle. For a particular geometry and material (plastic or cornea), the ablation efficiency factor is defined as the ratio of the ablation depth pattern on a spherical surface to the ablation depth pattern on a flat surface:

$$K = \frac{d_{SPH}}{d_{FLAT}} \quad , \tag{1}$$

where d is the ablation depth at each point. The effective ablation depth at each point of a curved surface can be predicted as $d_{eff} = d_{FLAT} \cdot K$. From a design point of view, *1/K* represents the correction factor (one at the center and higher than one at the periphery) by which the intended profile should be multiplied to compensate for the changes in ablation efficiency on

#111696 - $15.00 USD Received 20 May 2009; revised 27 Jul 2009; accepted 3 Aug 2009; published 14 Aug 2009

curved surfaces. The control algorithm should program d/K, in the laser, in order to obtain the desired pattern d ablated in the material.

For accurate estimations, it is essential that both ablations are registered, on the same coordinate center, which was estimated by fitting biconic surfaces to both ablation patterns. The selected radius of the base sphere subtracted from the ablated spherical surface elevation map was also critical in the assessment of the laser efficiency factor, as small discrepancies in the base sphere radius may result in slightly different ablation depths at the apex. As the ablation depth should be identical on flat and spherical surfaces in the center of the ablation, the base sphere radius was slightly refined (in steps of 0.05 mm) until that condition is reached. This refinement only affects the ablation patterns (estimated from spheres) in a few microns, but has a major impact on the fulfillment of the contour conditions (the efficiency factor is one in the center while the non-ablated zones are similar). The refinement needed in the base sphere is compatible with the small changes in the laser intensity observed between ablations and with the expected dilation effects on polymers [35] during the measurement.

2.5.3. Impact on cornea

The nominal ablation depth at the apex -provided by the system's software- is used to obtain a conversion factor between the ablation depth per pulse on plastic (Filofocon A) and corneal tissue. This factor changes with the laser, as it depends on fluence. The ideal ablation pattern in cornea (not affected by efficiency effects) can then be predicted by directly multiplying the ablation pattern on Filofocon by the plastic/cornea conversion factor.

To predict the actual shape of postoperative corneas, it is necessary to consider the geometry-related ablation efficiency factor for corneal tissue, which can be obtained from the ablation efficiency factor measured for plastic. According to the Beer-Lambert law, the etch rate (ablation depth per pulse) at each point of a flat surface should be given by $d_{FLAT}=(1/\alpha) \cdot ln\ (F_0 / Fth)$ where F_0 is the fluence of the laser, and α and Fth are the absorption coefficient and the ablation threshold of the material respectively. The reflection loss is already implicit in the experimental estimates of ablation properties (α and Fth) as they were obtained from regressions of the ablated depth at different laser fluences on flat surfaces (Ref. [32]). However, a reflection coefficient R, needs to be considered on non-flat surfaces [15]: $d_{SPH}=(1/\alpha) \cdot ln\ (F_0 R / Fth)$. That reflection coefficient depends on the surface geometry, incidence angle and refractive index. Then,

$$K = 1 + \frac{1}{\ln \frac{F_0}{Fth}} \ln R \quad . \tag{2}$$

The reflection coefficient R in this expression was obtained from the theoretical prediction of Jimenez et al. (ρ in Ref. [16]), but normalized to one, and therefore not including the reflection at the apex. The experimental (Eq. (1)) and theoretical (Eq. (2)) efficiency factors are normalized making both expressions for K equivalent. Operating with Eq. (2) for cornea K_C and Plastic, K_P we obtain:

$$K_C = 1 + \left(\frac{\ln R_C}{\ln R_P} \right) \left(K_P - 1 \right) \left(\frac{a_c}{a_P} \right) \quad . \tag{3}$$

Where $a_C = 1/ln(F_0 / Fth_C)$ and $a_P = 1/ln(F_0 / Fth_P)$, and the subscripts C and P stand for cornea and plastic respectively. The ablation thresholds Fth_C and Fth_P, and the refractive indices and surface geometry (through the reflection coefficients R_C and R_P) play a role in the conversion from the correction factor in plastic to the cornea. To calculate the correction factor for efficiency effects in cornea ($1/K_C$), we applied Eq. 3 point by point to the measured ablation efficiency factor in plastic. To estimate the postoperative corneal shape we multiplied the ideal ablation pattern in cornea obtained from the ablated flat plastic surfaces by the 2-D ablation efficiency factor in cornea. In this study we used the optical and ablation properties of Filofocon A reported in Ref. [32]: Fth_P=90 mJ/cm^2 and n=1.62. We used Fth_C=60 mJ/cm^2 and n=1.52 for the cornea.

#111696 - $15.00 USD Received 20 May 2009; revised 27 Jul 2009; accepted 3 Aug 2009; published 14 Aug 2009

2.5.4. Asphericities and spherical aberration

To assess the effect of the ablation pattern on the shape of the surfaces, we fitted the post-operative ablated spherical surfaces to conics and evaluated the change in asphericity [17]. To study the clinical relevance of this shape change, we simulated postoperative corneas applying the corneal ablation pattern calculated in the previous section to spherical corneas of 7.8 mm. We calculated the corneal asphericity and the corneal spherical aberration of these simulated postoperative corneas [36].

3. Results

3.1. Pre-operative shape measurements

The measured elevations of the pre-operative surfaces (plane or spherical) differed typically less than 1 micron (peak to peak) from their nominal shapes. The radius of curvature of the fitted spheres was also consistent with the nominal value (7.77±0.03 mm, on a 6.5-mm diameter). For diameters larger than 6.5-mm, a higher dispersion (up to 10 microns) was observed, more likely associated to the measurement technique than to the manufacture.

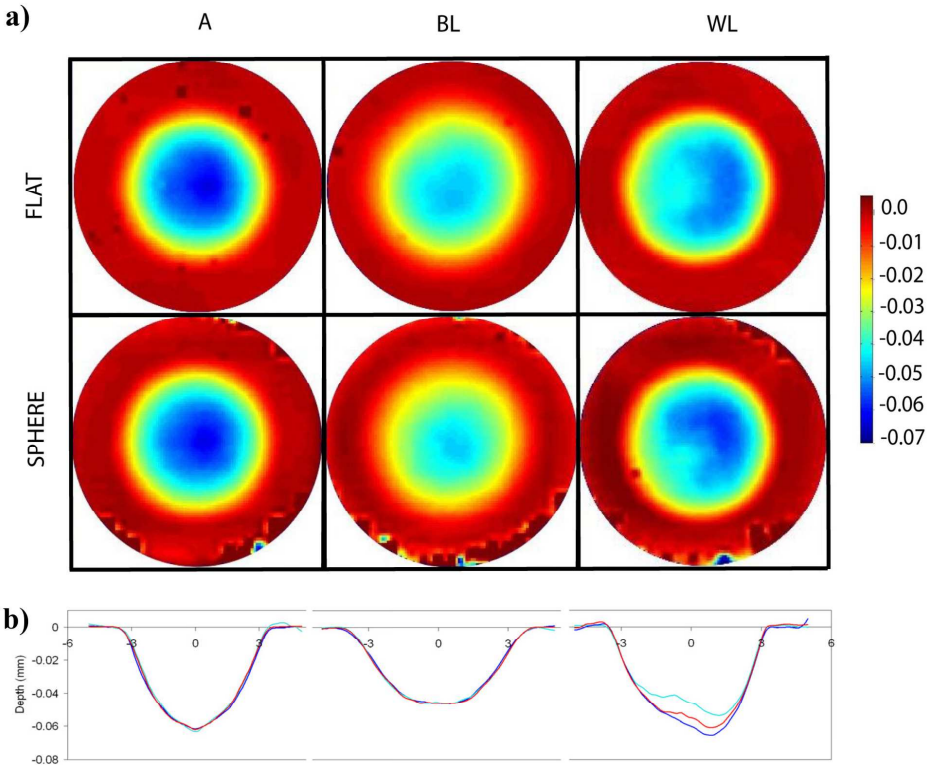

Fig. 3. (a) Examples of ablation patterns obtained from ablated flat and spherical surfaces for the three different lasers, and a correction of -9 diopters. (b) Horizontal sections of the ablation patterns on the flat surfaces (red lines), and other patterns obtained from different flat samples ablated on identical conditions (blue lines).

3.2. Ablation patterns on plastic

Figure 3 shows pairs (top row for flat surfaces, and bottom row for spherical surfaces) of representative ablation patterns for all lasers of the study. In all cases, a correction of –9 D was programmed in the laser.

The ablation patterns differed notably across lasers. While the Alcon and the Bausch & Lomb lasers provided highly symmetric patterns on both flat and spherical surfaces, the pattern delivered by the Wavelight laser showed asymmetries which were highly consistent

#111696 - $15.00 USD Received 20 May 2009; revised 27 Jul 2009; accepted 3 Aug 2009; published 14 Aug 2009

across measurements. Efficiency effects were responsible for a lower ablation depth in peripheral areas on spherical than on flat surfaces. This effect is notably larger in low fluence lasers (i.e. Bausch & Lomb laser) than higher fluence lasers (i.e. Alcon).

Figure 3 (b) shows horizontal profiles of the ablation patterns on flat surfaces. The red lines correspond to the examples shown 2-dimensionally, while the blue lines correspond to different repetitions corresponding to different samples. The high similarity of the laser profiles estimated from different ablated samples (with the same laser and similar conditions) illustrates the high repeatability, particularly of the Alcon and Bausch & Lomb lasers. When asymmetries were present, as found with the Wavelight laser, the differences across repeated measurements also increased. The asymmetries also appeared on different experimental sessions. Remarkably, the shape of the ablation profile and maximum ablation depth (on Filofocon A) differ substantially across laser platforms, for the same programmed refraction correction and optical zone.

3.3. Ablation efficiency factors on plastic

Figure 4 compares the ablation patterns for two of the lasers: Alcon (left side) and Bausch & Lomb (right side). Unlike Fig. 3 (b) where profile cross-sections of ablations on flat surfaces were plotted, Fig. 4 shows all the measured points in a radial plot, both for flat and spherical ablated surfaces (for -9D corrections on Filofocon A). The figure illustrates the large differences in ablation patterns between the two laser platforms. Both the ablation depth and the radial extension of the ablated zone are different. These two lasers are also different in terms of efficiency losses. The high fluence laser (Alcon, left side of Fig. 4) is practically free from efficiency losses. The ablation pattern from flat and spherical surfaces are almost identical for this laser, as the measured point to point difference in depth between ablation in flat and spherical surfaces (less than 2 microns) is of the order of the measurement accuracy. Theoretical calculations using the formulation of Anera et al. [15] for the particular geometry of the artificial eyes and the ablation properties of this material [32], predict a maximum difference of 1.1 microns.

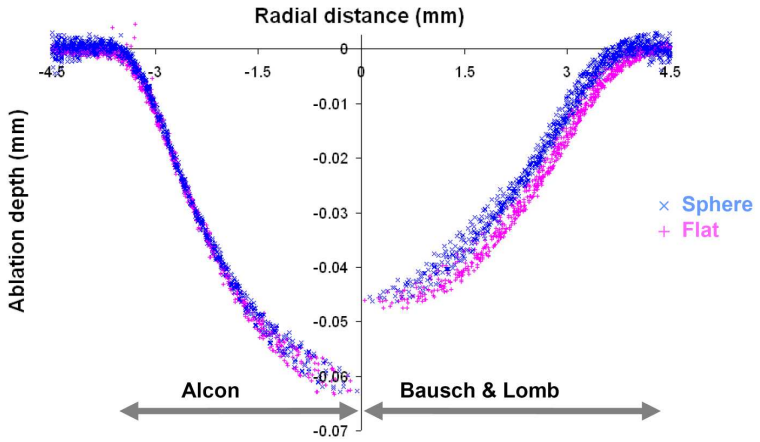

Fig. 4. Ablation patterns for two of the lasers: Alcon (left side) and Bausch & Lomb (right side). All the measured points are shown in radial plots, both for flat and spherical ablated surfaces (for -9D corrections on Filofocon A).

On the other hand, efficiency effects are clearly noticeable in the low fluence laser (Bausch & Lomb, right side of Fig. 4), as the ablation depth is lower on spherical than on flat surfaces. The difference between the ablation pattern on flat and on spherical surfaces is zero at the apex and also outside the ablation zone. There are systematic point to point differences, as high as 6.8 microns in the intermediate points (the theoretical prediction was 6.3 microns).

Figure 5 shows the measured ablation efficiency factor on Filofocon A (K, calculated from Eq. (1)) as 2-D maps and radial plots, for the Alcon (Fig. 5(a) and (b)) and Bausch & Lomb

#111696 - $15.00 USD Received 20 May 2009; revised 27 Jul 2009; accepted 3 Aug 2009; published 14 Aug 2009

(Fig. 5(c) and (d)) lasers. The square pattern observed in Fig. 5(a) is a trace of the profilometer trajectory. The red line in the 1-D plots (fig. 5 (b and c)) represents the theoretical ablation efficiency factor (*K,* from Eq. (2)) for the corresponding laser fluences (400 mJ/cm^2 and 120 mJ/cm^2 for the Alcon and Bausch and Lomb lasers, respectively), and using the ablation properties for Filofocon A that we have reported in a recent study [32].

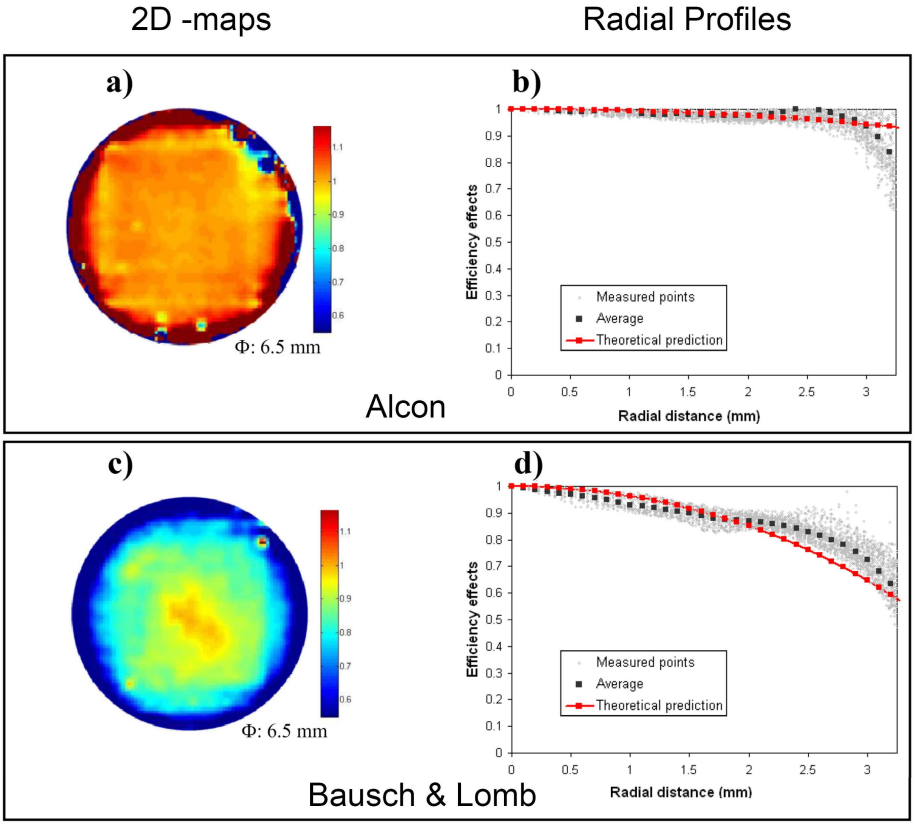

Fig. 5. Measured ablation efficiency factor in Filofocon A for the Alcon ((a) and (b)) and for the Bausch & Lomb laser ((c) and (d)). (a) and (c) show the efficiency effects at each point. (b) and (d) are radial profiles of all the measured points (gray). The black squares are the angular averages at each radial position. The red line represents the theoretical ablation efficiency factor for the corresponding laser fluences (400 mJ/cm^2 and 120 mJ/cm^2 for the Alcon and Bausch and Lomb lasers, respectively).

The experimental ablation efficiency factor at each radial distance from the apex (black squares) is obtained as an angular average of all the measured points (in gray). While the efficiency factor is practically 1 at all points for the high fluence laser (Alcon), it decreases significantly from the center to the periphery in the low fluence laser (Bausch & Lomb). For this laser (and Filofocon A) the effectiveness of ablation in the periphery of the optical zone is only 60%. The theoretical model captures the main experimental trends. The reported ablation efficiency factors were obtained from –9 D ablation patterns. We performed the same analysis on flat/spherical ablated surfaces with –3 D and –6 D corrections, and obtained similar results, although noise had a higher impact on the measured ablation depths.

3.4. Ablation patterns in cornea

We applied the depth conversion factor and the ablation efficiency factor from Eq. (3) to the ablation patterns measured on flat surfaces to predict the ablation pattern on corneal tissue. Figure 6 shows predictions of the ablation profiles on flat and spherical corneas (Fig. 6(b)), from the ablation profiles measured on flat plastic surfaces (Fig. 6(a)). The differences in the

#111696 - $15.00 USD Received 20 May 2009; revised 27 Jul 2009; accepted 3 Aug 2009; published 14 Aug 2009

ablation profiles as measured on Filofocon A between the Alcon and Bausch and Lomb lasers are clear in Fig. 6(a). In Filofocon, the Alcon laser (higher fluence) penetrates deeper in the plastic material and has a narrower ablation area while the Bausch & Lomb pattern on plastic is wider and shallower. The large differences in response between lasers are attenuated when the corresponding conversions to corneal tissue are applied (Fig. 6(b)). However, the ablation depth is significantly higher in cornea for the Bausch & Lomb laser, and the laser efficiency effects not negligible for this laser.

We also estimated the ablated volume from the predicted 2-dimensional corneal ablation patterns, for the Alcon and the Bausch & Lomb lasers, considering the experimentally measured ablation efficiency factor. Table 3 shows the ablation depth measured in Filofocon A, the nominal depth in cornea provided by the laser software, the corresponding depth conversion factor between cornea and Filofocon A, and the estimated ablated volume for the entire ablated area and within the optical zone.

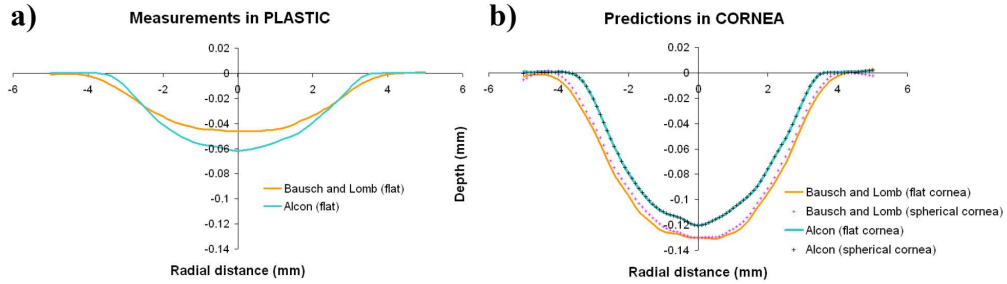

Fig. 6. Ablation profiles measured in Filofocon A flat surfaces (a) and predictions in corneal tissue (b) for flat and spherical surfaces.

It is interesting to note that the Zyoptix Tissue Saving algorithm of the Bausch & Lomb laser penetrates deeper in cornea and removes more material than the Standard optimized algorithm of the Alcon laser. Although the optical zone is the same in both lasers (6.5 mm) the ablated area is very different due to different design of the transition zones. Only 0.5% of the ablated volume is outside the optical zone with the Alcon laser (which has minimum transition zones), as opposed to 6.5% with the Bausch & Lomb laser. These ablated volumes were calculated considering the existing efficiency effects. If the efficiency effects were not considered (i.e. application on flat surfaces of the measured ablation profile, multiplied by the plastic-corneal tissue conversion factor) the ablated volume would be 5% larger for the Bausch & Lomb laser and 1% larger for the Alcon laser (within the optical zone in both cases).

Table 3. Ablation depths, depth conversion factors, and ablated volumes in cornea, for a -9 D correction.

	Alcon	Bausch & Lomb
Depth – Filofocon (μm)	62	47.8
Nominal Depth –Cornea (μm)	120.5	135
Conversion factor	1.94	2.82
Ablated corneal volume (μm^3)	$2.09 \cdot 10^9$	$2.76 \cdot 10^9$
Ablated volume within optical zone (μm^3)	$2.08 \cdot 10^9$	$2.58 \cdot 10^9$

3.5. Correction factors for efficiency effects in cornea

Figure 7 shows the correction factors for efficiency effects (*1/K*) predicted at each point of the human cornea for the Alcon (A) and the Bausch & Lomb (B) lasers. Figure 7(c) shows the radial average for both lasers, and the theoretical predictions. The efficiency effects are important for the Bausch & Lomb laser, as already seen in plastic, but not for the Alcon laser. Therefore, the correction factor increases from one (at the ablation center) to higher values

#111696 - $15.00 USD Received 20 May 2009; revised 27 Jul 2009; accepted 3 Aug 2009; published 14 Aug 2009

toward the periphery for the Bausch & Lomb laser, but remains almost flat for the Alcon laser. The radial average of the correction factor is well predicted by theory.

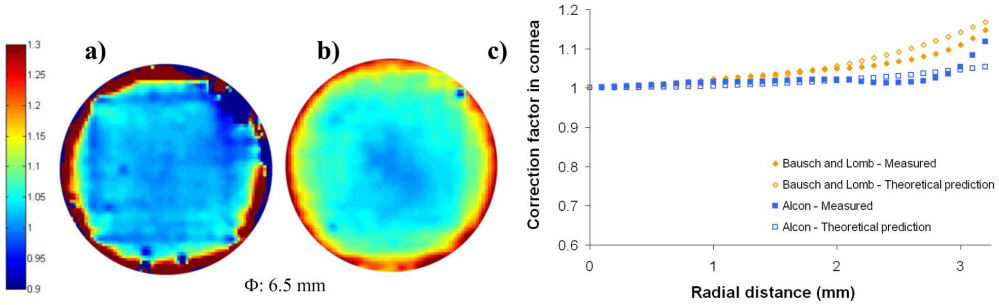

Fig. 7. Correction factor for efficiency effects in cornea estimated from the experimental measurements in Filofocon A. (a) Alcon. (b) Bausch & Lomb. c) Radial plots.

3.6. Optical outcomes in cornea

Figure 8 shows the asphericities obtained by fitting the ablated spheres of Filofocon A to conics, for the Bausch & Lomb (crosses) and the Alcon laser (diamonds). The figure also shows the asphericities found in a previous study [27] with a previous generation laser (Chiron Technolas 217c with PlanoScan). As the artificial eyes used in that study were made of PMMA, a conversion from PMMA to Filofocon A (considering the theoretical ablation efficiency factors for both materials) was applied to the measured ablation pattern. The post-operative asphericities with the new generation lasers are clearly below those obtained with previous generation lasers. However, the measured post-operative asphericity is still significantly different from zero (and positive).

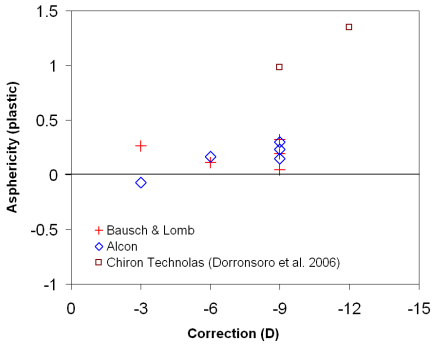

Fig. 8. Post-operative asphericities from Filofocon A ablated spheres for the Alcon (diamonds) and Bausch & Lomb lasers (crosses). The asphericities found in a previous study [27] with a previous generation laser (Chiron Technolas 217c with PlanoScan) are also shown (squares).

The average asphericity in post-operative Filofocon A for a -9 D correction was 0.23 for the Alcon laser, and 0.19 for the Bausch & Lomb laser. When the ablation pattern was transferred to the cornea (considering the corresponding efficiency effects) we obtained a post-operative asphericity of 0.40 for the Alcon laser and 0.71 for the Bausch and Lomb. The corresponding spherical aberration in cornea [36] was 0.47 μm for the Alcon laser, and 0.61 μm for the Bausch & Lomb laser. The spherical aberration of an ideal spherical cornea of 7.8 mm is 0.49 microns.

4. Discussion

This work further develops the use of plastic model corneas to obtain precise quantitative evaluation of the ablation patterns provided by refractive surgery laser systems [27]. The depth patterns are measured on plastic, which can provide an accurate calibration of the laser

#111696 - $15.00 USD Received 20 May 2009; revised 27 Jul 2009; accepted 3 Aug 2009; published 14 Aug 2009

system. Furthermore, the combination of precise profilometric measurements on plastic surfaces, and knowledge of the ablation and optical properties of the plastic material provides estimations of the ablation pattern on cornea, considering all physical effects, and excluding biomechanical factors. In a previous study of the ablation properties of Filofocon A [32] we showed that a depth pattern measured on this material can be transformed into a laser spot distribution (considering the fluence of the laser), which can be used to predict depth patterns in cornea, provided that the number of pulses is sufficiently high -as is it the case within the optical zone (see discussion of Ref. [32] for details)-.

The fact that the ablation response of Filofocon A is well predicted by the Beer-Lambert law, for the range fluences and number of pulses used in refractive surgery [32] allows an accurate characterization of the ablation pattern on plastic. On the other hand, the estimations of the ablation pattern on cornea are accurate within the limitations of the blow-off model in corneal tissue (Beer-Lambert Law) and the accuracy of the optical and ablation parameters. The estimation of the ablation profile on cornea from the measurement of the ablation profile on plastic could be further sophisticated using more complex ablation models [19, 20], or parameters for the cornea, as dynamic coefficients [37].

The geometrical efficiency effects depend on the geometry of the surface on which the corrected ablation pattern is going to be applied. Therefore, strictly speaking, the estimated correction factor to be applied on a spherical surface would be different to that estimated for a conic surface. We performed simulations to quantify the error induced by considering a correction factor calculated for spherical corneas on conic corneas. We found, for a cornea of asphericity -0.4 (upper bound of asphericity in normal corneas) a mean underestimation of 0.21% in the energy applied to the cornea, and a maximum deviation (in the periphery of a 6.5-mm optical zone) of -1.01%. These values are of negligible clinical relevance. In the case of a retreatment of a highly aspherical post-surgical cornea (asphericity = 1), the correction factor for spherical surfaces overestimates the energy applied to the conic cornea (mean 0.63%, maximum 3.31% in the periphery of the ablation).

Equation (1) considers all the possible efficiency effects of the laser in plastic (K_P), and an accurate characterizations of the lasers, as the geometry of the plastic surfaces used (and therefore R_P) are well known. The maximum accuracy of the correction factors in cornea (K_C) can obtained when the geometry of individual corneas are taken into account (and not only a generic corneal geometry) in the reflection coefficient R_C used in the conversion from plastic to cornea.

Previous studies were limited by the use of videokeratoscopy to assess the elevation maps of pre- and post-operative spherical surfaces from which the ablation patterns are computed. The use of high resolution non-contact optical profilometry allows mapping both flat and spherical surfaces with the same instrument and with high accuracy (less than 1 micron), without the need of the slight polishing of post-ablated surfaces, required to achieve proper reflection in videokeratoscopy. This procedure allows accurate point-by-point assessment of the ablation efficiency factor of the laser, using the ablation pattern measured in pairs of flat and spherical surfaces ablated consecutively under similar conditions. The 2-D correction factor for efficiency effects can be applied to any ablation algorithm programmed on a given laser platform.

Our previous study evaluated standard ablation profiles on PMMA. The current study uses the recently proposed Filofocon A material, which we showed to have more suitable ablation properties [32]. We used this new model to evaluate the ablation patterns produced by three state-of-the-art refractive surgery laser platforms. We performed a detailed comparison between two of the lasers (Alcon and Bausch & Lomb, with very different nominal fluences). We found marked differences across lasers in the ablation pattern measured in plastic (Fig. 4), ablation efficiency factors (Fig. 5), predicted post-operative corneal shape, (Fig. 6), correction factor in cornea (Fig. 7), post-operative asphericities (Fig. 8), ablated volume and spherical aberration in plastic and cornea.

#111696 - $15.00 USD Received 20 May 2009; revised 27 Jul 2009; accepted 3 Aug 2009; published 14 Aug 2009

Toward an optimized ablation pattern

A comparison of the optical outcomes (both in plastic and cornea) following myopic ablation using new generation and older laser platforms suggest that current ablation patterns have been conveniently optimized to reduce the induction of spherical aberration in the new generation lasers, although there is still room for improvement (Fig 8, in Filofocon A). Our predictions suggest that the optimized algorithms are still inducing some change in the asphericity of the cornea (0.40 for the Alcon laser and 0.71 for the Bausch & Lomb, for -9 D correction), although much less than the one reported (1.44 for -9 D) with a previous generation laser and the previous plastic model of Ref. [27]. We can also compare the relative impact of laser efficiency effects and ablation pattern design in the post-operative asphericity. When ablation efficiency effects are cancelled (simulating post-operative corneas by subtraction of the ablation pattern obtained from ablated flat surfaces) we found similar post-operative asphericities with both lasers (~0.35). This suggests that the increase in asphericity for the Alcon laser arises primarily from the ablation pattern while for the Bausch & Lomb laser the efficiency effects account for most of the increase in asphericity.

Ablations on Filofocon A: a method for laser calibration

One especially interesting feature of Filofocon A as a model for refractive surgery is its relatively high sensitivity to fluence changes, compared to PMMA and corneas, due to the combination of its high threshold fluence (90 mJ/cm^2) and high refractive index at 193 nm (1.62), which increases reflection. As a result, the efficiency effects and the associated induced asphericity are more apparent in Filofocon A than in corneas or PMMA, making them easier to measure. On the other hand, the laser penetrates much deeper in cornea than in Filofocon A, and as a result the effects associated to the shape of the ablation pattern are more important in cornea than in Filofocon.

The procedure described in this study can be used to check the calibration state and the performance of individual units of refractive surgery laser systems. The entire ablation pattern in the cornea can be estimated from these measurements. We observed important deviations from rotational symmetry in one of the lasers (Fig. 3, Wavelight laser). The asymmetries appeared both on flat and spherical surfaces (and also with both Q parameters tested) and the location of the irregularity changed across repeated ablations. Validation tests (involving repeated profilometric measurements of the same samples at different orientations) proved that the irregularities were a consequence of the ablation process and not of the measurement. Decentration and alignment effects were discarded as a possible cause for the observed asymmetries, as they should not affect the ablation pattern on flat surfaces. Shielding effects by ablation plume or debris ejected during the ablation [38] were the most likely cause for the asymmetry, which may have been produced by insufficient air suction, perhaps as a consequence of the filter wheel position (Fig. 2). A retrospective analysis of corneal topographies in patients operated with this laser unit did not show important asymmetries, confirming this hypothesis. It is important to note that the procedure of estimating the ablation patterns in cornea is based on the assumption that the ablation pattern in flat surfaces of plastic is created by the superposition of a set of equal spots. If the fluence varies (due to shielding, obscuration, etc), the methodology can detect these changes, but the effects in cornea cannot be correctly quantified. In most cases the assumption of superposition holds, and therefore the model can be used to assess the ablation profile programmed on the laser.

5. Conclusions

Plastic (Filofocon A) artificial model eyes have proven useful to assess the outcomes of different refractive surgery laser platforms and algorithms, for a precise calibration of the lasers and to calculate experimental correction factors of efficiency effects.

Different state-of-the-art optimized laser platforms, programmed to produce the same myopic corrections in eyes, showed very different ablation profiles on plastic corneas (30%

#111696 - $15.00 USD Received 20 May 2009; revised 27 Jul 2009; accepted 3 Aug 2009; published 14 Aug 2009

differences in ablation depths for a -9 D myopic correction) which translated in 34% differences in corneal tissue volume differences.

The ablation efficiency factor varied also substantially across lasers, as estimated from the ratios of the ablation profile on flat and spherical plastic surfaces. For a laser fluence of 120 mJ/cm^2 the efficiency loss (for Filofocon A) was 6.5% at 2.5 mm from the corneal apex, while at 400 mJ/cm^2 this effect was practically negligible.

Both the ablation algorithm design and the strategy of compensation for the ablation efficiency factors contributed to the optical outcomes. The estimated post-operative corneal asphericity is half with the new generation laser algorithms than with non-optimized algorithms (for -9 D correction), but still not negligible. Plastic artificial eye models allow a systematic evaluation of the ablation profile and of the correction factor for efficiency effects, which is essential to further improve ablation algorithms to avoid increase of corneal asphericity (and spherical aberration), which still occurs from purely physical factors

Acknowledgments

We thank Benjamín Alonso-Fernández (University of Salamanca) for support in the initial stages of this study. We thank Jan Siegel (IO-CSIC), José Antonio Sánchez-Gil (IEM - CSIC), and Juan Francisco Vega (IEM - CSIC) for useful discussions. We thank Cristina Cadevall (CD6-UPC) for technical support with profilometry and customization of the Sensofar instrument. Ablations were performed in Madrid, in the following clinical sites: Clínica Baviera, Clínica Novovision, and Clínica Oculaser. Special thanks to Dr. Ramón Gutierrez and César Villa (Novovision), Gemma Álvarez (Clínica Baviera), Carmen Garcia Franco (Oculaser), Santiago Medrano (Wavelight), Saskia Aguado (Bausch & Lomb), and Félix Tobar (Alcon). This research was Supported by grants #FIS2005-04382 and #FIS2008-02065 (Ministerio de Ciencia e Innovación, Spain) and EURYI-05-102-ES (EUROHORCS-ESF). Support from Unidad Asociada IO-CSIC/IOBA-Universidad de Valladolid is also acknowledged.

#111696 - $15.00 USD Received 20 May 2009; revised 27 Jul 2009; accepted 3 Aug 2009; published 14 Aug 2009